This is the Pre-Published Version.

The following publication W. A. Gemechu et al., "Dual Polarization Nonlinear Frequency Division Multiplexing Transmission," in IEEE Photonics Technology Letters, vol. 30, no. 18, pp. 1589-1592, 15 Sept.15, 2018 is available at https://doi.org/10.1109/LPT.2018.2860124.

Dual Polarization Nonlinear Frequency Division Multiplexing Transmission

Wasyhun A. Gemechu, Tao Gui*, Jan-Willem Goossens, Mengdi Song, Stefan Wabnitz, Hartmut Hafermann, Alan Pak Tao Lau, Mansoor I. Yousefi, and Yves Jaouën

***Abstract*—We experimentally demonstrate dual-polarization nonlinear frequency division multiplexing using the continuous spectrum in 1680 km of normal dispersion fiber, at the net data rate of 25.6Gbit/s. NFDM exhibits a gain of 0.4 dB in Q-factor and 1 dB in total launch power when compared with burst mode OFDM. DGD penalties are shown to be negligible in NFDM transmission.**

***Index Terms*— Nonlinear Fourier transform, nonlinear frequency division multiplexing, normal dispersion, polarization division multiplexing**

I. Introduction

n current long haul optical communication systems, the main Ilimiting factor to channel rate and transmission reach is channel interference owing to Kerr nonlinearity [1]. Several nonlinearity mitigation techniques, e.g., digital optical phase conjugation [2], Volterra series transfer function [3], and digital back propagation [4], have been proposed to combat fiber nonlinearities. However, the practical Q-factor performance gain was limited to ~0.5 – 1 dB, owing to noise-nonlinearity interactions and cross-phase modulation (XPM) [3,5].

A different nonlinearity mitigation technique that has gained attention in recent years is nonlinear frequency-division multiplexing (NFDM) [6]. In this approach, information is encoded by exploiting the nonlinear Fourier transform (NFT). In this way, one generates nonlinear spectral channels that propagate independently, in principle allowing for interference-free communications.

Several experimental demonstrations of NFDM have been reported: these experiments employed transmission fibers operating either in the anomalous or in the normal dispersion regime, respectively. In the former case, the nonlinear spectrum consists of continuous and discrete components, which can be separately [7-8,9] or jointly [10] modulated. In the latter case, there is no discrete spectrum and only the continuous spectrum can be modulated [11]. By using the NFDM approach, Q-factor gains of up to 1 dB over transmission schemes using linear frequency division multiplexing were reported.

More recently, it has been proposed that NFDM can be combined with polarization division multiplexing (PDM) for transmission based on continuous spectrum modulation [12]. The experimental demonstration of dual-polarization eigenvalue communication over 373.5 km was reported [13].

In this Letter, we experimentally demonstrate dual-polarization NFDM of the continuous spectrum with a normal dispersion transmission fiber. We obtain a 0.4 dB Q-factor (1 dB in SNR) gain when compared with OFDM, for transmissions over 1680 km at the net data rate of 25.6 Gbit/s, when taking into account the guard interval duration.

II. Theory of PDM-NFDM

When neglecting polarization mode dispersion (PMD), vector pulse propagation in periodically amplified optical fiber links can be described by the path-averaged lossless Manakov equation [14]

$$\frac{\partial \mathbf{A}}{\partial Z} = i\frac{\beta_2}{2}\frac{\partial^2 \mathbf{A}}{\partial t^2} - i\gamma\|\mathbf{A}\|^2\mathbf{A} \tag{1}$$

Here $\mathbf{A} = A_k, k = 1,2$ is the Jones vector describing complex envelopes of the electrical field in the two polarizations, $Z \in [0, L]$ is the transmission distance, t is a retarded time, β_2 is the dispersion coefficient, and γ is the effective nonlinearity coefficient [15].

We may express (1) in the usual dimensionless units

$$\mathbf{q} = \frac{\mathbf{A}}{A_0}, \quad \tau = \frac{t}{T_0}, \quad z = \frac{Z}{L_D}, \tag{2}$$

where

$$L_D = 2T_0^2/|\beta_2|, \quad A_0 = \sqrt{2/\left(\tfrac{8}{9}\gamma L_D\right)},$$

We obtain the dimensionless Manakov equation

$$i\frac{\partial \mathbf{q}}{\partial z} = \frac{\partial^2 \mathbf{q}}{\partial \tau^2} - 2s\|\mathbf{q}\|^2\mathbf{q} \tag{3}$$

with $s = \pm 1$, where $s = 1$ corresponds to the normal

S.W. was supported by the Ministry of Education and Science of the Russian Federation (14.Y26.31.0017) and T. Gui. was supported in part by general research grant council, Hong Kong under project number PolyU152116/15E.

W. A. Gemechu, T. Gui, J.-W. Goossens, M. Song, M. I. Yousefi and Y. Jaouën are with *LTCI, Telecom ParisTech, Université Paris-Saclay, 75634 Paris, France* (e-mail: tao.gui@connect.polyu.hk).

W. A. Gemechu and S. Wabnitz are with Dipartimento di Ingegneria dell'Informazione, Università degli Studi di Brescia, 25125, Brescia, Italy (email: w.gemechu@unibs.it); S. Wabnitz is also with Novosibirsk State University, Novosibirsk 630090, Russia.

T. Gui and A. P. T. Lau are with Photonics Research Centre, Department of Electrical Engineering, The Hong Kong Polytechnic University, Hung Hom, Kowloon, Hong Kong.

J.-W. Goossens and H. Hafermann are with Mathematical and Algorithmic Sciences Lab, Paris Research Center, Huawei Technologies France, France.

dispersion regime. Here T_0 is a free parameter.

Eq. (3) can be represented by means of the so-called Lax equation

$$\frac{\partial \hat{L}}{\partial z} = \left[\hat{M}, \hat{L}\right] \tag{4}$$

where the $\hat{L}$ and $\hat{M}$ are 3x3 matrix operators [14]. For example,

$$\hat{L} = i\begin{pmatrix} \frac{\partial}{\partial t} & -q_1 & -q_2 \\ sq_1^* & -\frac{\partial}{\partial t} & 0 \\ sq_2^* & 0 & -\frac{\partial}{\partial t} \end{pmatrix} \tag{5}$$

The eigenvalues λ of $\hat{L}$ are invariant upon fiber propagation and the nonlinear Fourier coefficients a, $b_1$and b_2 are computed from their eigenvectors [14]. The continuous spectrum is then given by

$$\hat{\mathrm{q}}_k(\lambda, z) = \frac{b_k(\lambda, z)}{a(\lambda, z)}, \lambda \in \Re \tag{6}$$

To numerically compute the NFT, we use the Ablowitz-Ladik discretization of $\hat{L}$, and apply the discrete layer peeling method for the inverse NFT (INFT) [12]. In the absence of noise, the input-output relation for the signal NFT reads as

$$NFT(\mathbf{q}(\tau, L)) = H(\lambda, L) \times NFT(\mathbf{q}(\tau, 0)) \tag{7}$$

where $H = \exp\left(-is4\lambda^2 L\right)$ an all-pass-like channel filter.

In PDM-NFDM (PDM-OFDM) transmissions, each subcarrier is modulated and multiplexed on the nonlinear (linear) spectrum by using the M-QAM modulated symbol ($c_{l,m}^k$) format. A signal in the k^{th}-polarization is formed as

$$\mathbf{U}_k(\lambda, 0) = P_{\max} \sum_{l=1}^{N_{sub}} \sum_{m=1}^{N_{symbol}} c_{l,m}^k \frac{\sin(\lambda - lW_0)}{(\lambda - lW_0)} e^{i\lambda mT} \tag{8}$$

where $P_{max}, N_{sub}, N_{symbol}, W_0$ and T represent the peak power per polarization, sub-carrier number, number of symbols, sub-carrier spacing and the total symbol duration, respectively and $\lambda = \pi f$, where f is frequency. A signal in the **U**-domain is then mapped into the nonlinear spectral domain $\hat{\mathbf{q}}$ according to

$$\hat{\mathbf{q}}(\lambda, 0) = \sqrt{1 - e^{-|\mathbf{U}(\lambda,0)|^2}} \frac{\mathbf{U}(\lambda, 0)}{|\mathbf{U}(\lambda, 0)|} \tag{9}$$

This step enforces the fundamental constraint $|\hat{\boldsymbol{q}}| < 1$. Finally, the time domain signal is computed as $\boldsymbol{q}(t, 0) = \mathrm{INFT}(\hat{\boldsymbol{q}}(\lambda, 0))$ before its injection into the fiber. Note that INFT processing acts on each symbol separately. In OFDM, one directly generates the input signal $\boldsymbol{U}(f)$ as eq.(8).

III. Experimental Setup

The $32 \times 0.5GBd$ NFDM/OFDM symbols in each polarization consist of 32 orthogonal subcarriers modulated with 16QAM complex symbols at the transmitter. The transmitted symbol blocks include synchronization symbols (SS), polarization separation symbols (PSS), training symbols (TS), and data symbols, as shown in Fig. 1. PSS symbols are generated using OFDM with cyclic-prefix for MIMO channel separation. Whereas TS and data symbols are defined in the NFT domain, and the prior used for MIMO channel equalization.

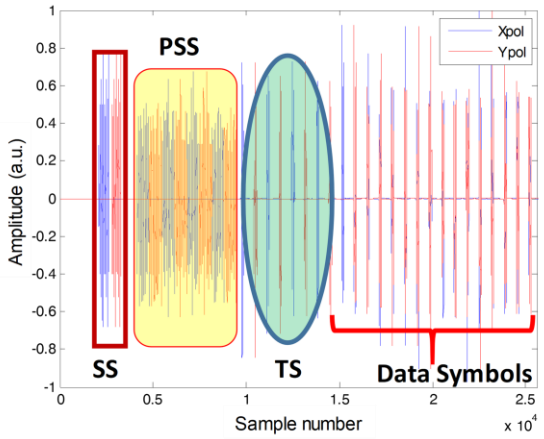

Fig. 1. Data structure of real part of 16QAM PDM-NFDM/OFDM.

The NFDM symbols are oversampled by a factor 8, thus increasing the sampling frequency to 512Gs/s, for accurate computation of the nonlinear spectrum. We compute $\boldsymbol{u} = \mathcal{F}^{-1}(\boldsymbol{U})$, where $\mathcal{F}$ stands for FFT, in order to introduce a guard band of 8 ns, to satisfy the vanishing boundary conditions of the Zakharov-Shabat spectral problem [14] in time domain (i.e., a total symbol duration of ~10 ns). Since NFT processing is applied to each data symbol separately, guard bands added to both front and end of NFDM/OFDM symbols prevent inter-burst interference, and accommodate symbol broadening due to the combined action of dispersion and nonlinearity during fiber propagation. Prior to mapping user data into the NFT domain according to (9), we compute $\boldsymbol{U} = \mathcal{F}(\boldsymbol{u})$. Time domain NFDM symbols are computed by the INFT algorithm. Four of the subcarriers are used as pilot tones for laser phase noise estimation. To perform dual-polarization transmission, we use a polarization division multiplexing emulator (PDME). As shown in the inset in Fig. 2, the single complex I/Q modulator serially generates both X and Y polarization data as follows: $q_y^1, q_x^1, q_y^2, q_x^2, \ldots$. Next, the PDME splits the two orthogonal polarization components of the signal, delays the Y component by one symbol, and recombines them. As a result, NFDM symbols not involving the same serial number in the two polarizations (as indicated by red circles in Fig.2) are discarded at the receiver.

Fig. 2 shows the experimental setup of our 16GHz PDM-NFDM/OFDM transmission system: yellow boxes indicate the additional DSP block for NFDM. The NFDM signal is resampled to 64 GS/s before being loaded into the arbitrary waveform generator (AWG). The optical signal is generated by using a complex I/Q modulator. Linear adaptation is employed to pre-equalize only the amplitude imperfection of the transmitter and receiver.

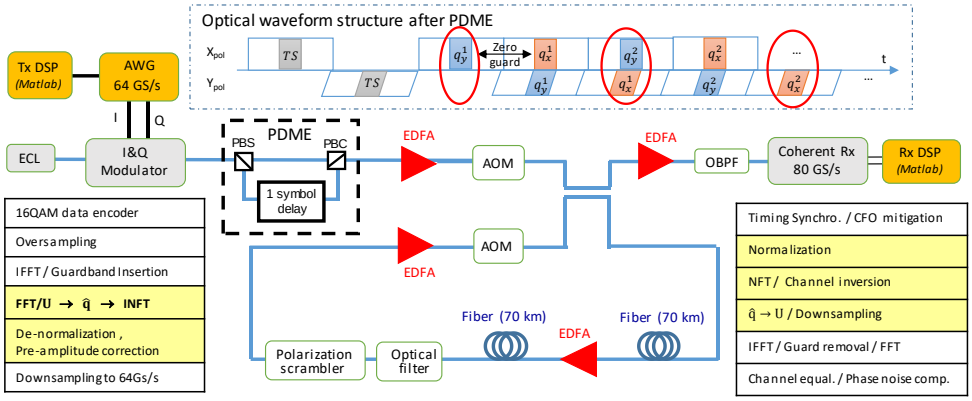

Fig. 2. Experimental setup, PDM-NFDM data stream structure and offline Tx/Rx DSP

The I/Q modulator output passes through the PDME with 1 symbol time delay (~10 *ns*), is amplified and then launched into a negative dispersion fiber designed for submarine transmissions (TW-SRS fiber, α = 0.2 dB/km, D = -4.66 ps/nm/km and S_{eff} = 53.5μm^2). The transmission link within the recirculating loop consists of two 70-km fiber spans and two EDFAs (NF = 5.5 dB). An optical band-pass filter (OBPF) with a 3 dB bandwidth of 1 nm is used inside the loop, to suppress out-of-band ASE noise. A polarization scrambler is included in the loop, to randomize the polarization state after each loop. An external cavity laser (ECL) ($\Delta\nu \approx 100kHz$) is used both as the optical carrier, and the local oscillator at the transmitter and receiver, respectively. The signal is detected by an intradyne coherent receiver, and sampled by a real time 80GS/s sampling oscilloscope. The sampled signal is analyzed by offline digital signal processing (DSP), whose structure is also shown in Fig. 2.

At the receiver, after timing synchronization and carrier frequency offset (CFO) compensation using synchronization symbols, the received samples are separated in time blocks. The PSS symbols are separated, and chromatic dispersion compensation applied to them. The compensated PSS symbols are then used to separate the two states of polarization and equalize the amplitude distortion arising from transmission imperfections. NFDM symbols are then normalized for carrying out the NFT operation. Here the wrongly combined symbols are dropped as shown in the inset of Fig. 2. Channel inversion on the received $\hat{\boldsymbol{q}}_i$ is done by using a single-tap equalizer, to compensate for both dispersion and nonlinearity jointly according to (7), and translated into the **U**-domain by inverting (9). After removing the guard bands in time domain, and resampling in frequency domain, the received symbols are compensated for residual channel amplitude and phase distortions in the nonlinear frequency domain by using NFT training symbol-aided MIMO channel estimation. We exploit the same training symbols to correct potential synchronization timing errors. Synchronization timing errors manifest themselves as a frequency dependent phase shift, that can be compensated by using the time shift property of the NFT:

$$\mathbf{q}(t-\tau) \leftrightarrow e^{-2i\lambda\tau}\hat{\mathbf{q}}(\lambda) \qquad (12)$$

Rx DSP was thus optimized to minimize phase error, which is the key for performance gain in NFDM transmissions. The pilot-aided laser phase noise estimation was done in the NFT domain, because any phase variation that affects the time domain signal directly translates into phase noise in the NFT domain. Finally, maximum likelihood detector based symbol decision and bit error rate (BER) calculation were performed. In back-to-back, the same error vector magnitude (EVM) value of 12% was obtained for SP- and PDM-NFDM, which means that there were no PDM implementation issues.

IV. Experimental Results

In Fig. 3, typical examples of transmitted PDM NFDM symbols are presented. The signal energy in the decaying tails increases with input power, and it is taken into account in INFT processing. The received constellations at -3 dBm optimal launch power are presented in Fig. 4. In Fig.5 we compare the Q-factor of single- and dual-polarization NFDM with OFDM, for the same baud-rate and input launch burst power. The Q-factor is calculated from the BER measurements. The BERs values are almost identical for both polarizations. For a fair comparison between NFDM and OFDM, we do not include a cyclic prefix in OFDM data symbols: therefore, chromatic dispersion equalization is applied before the OFDM receiver. The input launch power reported in Fig.5 corresponds to the average launch power in the fiber including guard bands.

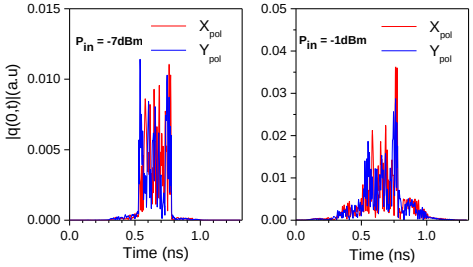

Fig 3: Examples of PDM-NFDM time domain symbols.

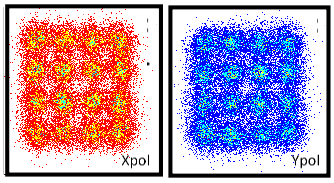

Fig 4: Received constellations at -3dBm for PDM-NFDM.

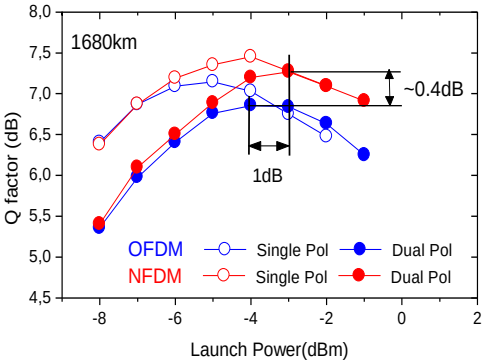

Fig. 5. NFDM and OFDM results in SP- and PDM-NFDM.

Fig. 5 shows that optimal performance is obtained at -4 dBm for PDM-OFDM, and -3 dBm for PDM-NFDM, with a peak Q-factor of 6.84 dB and 7.25 dB, respectively. For SP-OFDM and SP-NFDM, optimal Q-factors of 7.1 dB and 7.5 dB are obtained, at launch powers of -5 dBm and -4 dBm, respectively. At relatively low powers, we observe a ~2 dB power difference between SP and PDM-NFDM, in place of 3dB as expected in the linear regime. This power difference is reduced at high input powers, owing to increased signal-noise interactions and numerical errors in the INFT/NFT algorithm. In fact, at high input powers the NFDM signal has long decaying tails and a high peak to average power ratio when compared with its low power counterpart, as shown in Fig. 3. This contributes to the performance degradation. We observed that higher sampling rates at the Rx, and synchronization timing error related phase corrections led to significantly improved NFDM transmission performance. In our experiments, polarization impairments such as polarization mode dispersion, polarization dependent loss and differential group delay (DGD) were not compensated.

To estimate the effect of DGD on the performance of NFDM and OFDM, we introduce an extra time delay at the AWG between successive symbols. This results in temporal mismatch between the two polarizations at the PDME output. We reduced the propagation distance to 980km, in order to increase the Q-factor, thus allowing for more accurate assessment of DGD effects. Fig. 6 shows that DGD has a higher impact on the Q-factor for PDM-NFDM than for PDM-OFDM. However, for typical PMD parameters less than 0.1 ps/√km, the Q-factor penalty caused by DGD is insignificant for the transmission distance of our experiments.

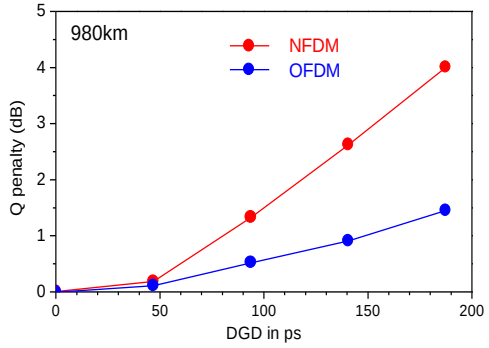

Fig. 6: Q penalty induced by DGD

V. Conclusion

We demonstrated PDM-NFDM transmission by using the continuous spectrum in a normal dispersion optical fiber. Compared with PDM-OFDM, a Q-factor gain of 0.4 dB (OSNR gain of 1 dB) was obtained. The relative performance of NFDM with respect to OFDM is expected to be further improved by compensating polarizations impairments, by reducing numerical errors in the NFT/INFT algorithms at high powers, by PAPR reduction, and by performing Tx-Rx adaptation.

Acknowledgment

The authors thank Nicolas Brochier and Erwan Pincemin of Orange Labs, France, for providing the TW-RSR fiber.

References

[1] R.-J. Essiambre, G. Kramer, P. J. Winzer, G. J. Foschini, and B. Goebel, "Capacity limits of optical fiber networks," J. Lightwave Tecnol., vol. 28, no. 4, pp. 662–701, Feb. 2010.

[2] X. Chen, X. Liu, S. Chandrasekhar, B. Zhu, and R. W. Tkach, "Experimental demonstration of fiber nonlinearity mitigation using digital phase conjugation," in *Proc. OFC*, Los Angeles, CA, USA, Mar., 2012, paper OTh3C.1.

[3] A. Amari, O. A. Dobre, R. Venkatesan, O. S. Kumar, P. Ciblat and Y. Jaouën, "A survey on fiber nonlinearity compensation for 400 Gbps and beyond optical communication systems," IEEE Commun. Surv. Tutorials, vol. 19, no. 4, pp. 3097-9113, Nov. 2017.

[4] E. Ip and J. Kahn, "Compensation of dispersion and nonlinear impairments using digital backpropagation," J. Ligthwave Technol. vol. 26, no. 20, pp. 3416–3425, Oct. 2008.

[5] R. Dar and P. J. Winzer, "Nonlinear interference mitigation: Methods and potential gain," J. Ligthwave Technol. Vol. 35, no. 4, pp. 903–930, Feb. 2017.

[6] M. I. Yousefi and F. R. Kschischang, "Information transmission using the nonlinear Fourier transform," Part I-III, IEEE Transactions on Information Theory, vol. 60, no. 7, 4312-4328, Apr. 2014.

[7] S. T. Le, I. D. Philips, J. E. Prilepsky, P. Harper, A. D. Ellis, S. K. Turitsyn, "Demonstration of nonlinear inverse synthesis transmission over transoceanic distances," J. Ligthwave Technol., vol. 34, no. 10, pp. 2459-2466, May 2016.

[8] S. T. Le and H. Buelow, "64 × 0.5 Gbaud Nonlinear Frequency Division Multiplexed Transmissions With High Order Modulation Formats," J. Ligtwave Technol., vol. 35, no. 17, pp. 3692-3698, Sept. 2017.

[9] T. Gui, C. Lu, A. P. T. Lau and P. K. A. Wai, "High-order modulation on a single discrete eigenvalue for optical communications based on nonlinear Fourier transform," Optics Express, vol. 25, no. 17, pp. 20286-20297, Aug. 2017.

[10] S. T. Le, V. Aref and H. Buelow, "Nonlinear signal multiplexing for communication beyond the Kerr nonlinearity limit," Nat. Photonics, vol. 11, no. 9, pp. 570–576, July 2017.

[11] W. A. Gemechu, M. Song, Y. Jaouën, S. Wabnitz, and M. I. Yousefi, "Comparison of the Nonlinear Frequency Division Multiplexing and OFDM in Experiment," *in Proc. ECOC*, Gothenburg, Sweden, Sept. 2017, Paper W.3. C.4.

[12] J.-W. Goossens, M. I. Yousefi, Y. Jaouën, and H. Hafermann, "Polarization-division multiplexing based on the nonlinear Fourier transform," Optics Express, vol. 25, no.22, pp.26437–26452, Oct. 2017.

[13] S. Gaiarin, A. M. Perego, E. P. da Silva, F. D. Ros, and D. Zibar, "Dual-polarization nonlinear Fourier transform-based optical communication system," Optica, vol.5, no.3, pp. 263-270, Mar. 2018.

[14] S. V. Manakov, "On the theory of two-dimensional stationary self-focusing of electromagnetic waves," Soviet Physics-JETP, vol. 38, no. 2, pp. 248–253, Aug. 1974.

[15] S. T. Le, J. E. Prilepsky, and S. K. Turitsyn, "Nonlinear inverse synthesis technique for optical links with lumped amplification," Optics Express, vol. 23, no. 7, pp. 8317–8328, Mar. 2015.